PHYSICAL REVIEW B **87**, 161105(R) (2013)

Electronic structure of vacancy-ordered iron-selenide $K_{0.5}Fe_{1.75}Se_2$

Chao Cao[1,*] and Fuchun Zhang[2,†]

[1]*Condensed Matter Group, Department of Physics, Hangzhou Normal University, Hangzhou 310036, China*

[2]*Department of Physics, Zhejiang University, Hangzhou 310027, China*

(Received 20 February 2013; revised manuscript received 19 March 2013; published 11 April 2013)

The electronic structure of the vacancy-ordered $K_{0.5}Fe_{1.75}Se_2$ iron-selenide compound (278 phase) is studied using the first-principles density functional method. The ground state of the 278 phase is stripelike antiferromagnetic, and its bare electron susceptibility shows a large peak around (π,π) in the folded Brillouin zone. Near the Fermi level, the density of states is dominated by the Fe-3*d* orbitals, and both electronlike and holelike Fermi surfaces appear in the Brillouin zone. An unfolded band structure shows limited similarities to a hole-doped 122 phase. With 0.1*e* electron doping, the susceptibility peak is quickly suppressed and broadened, while the two dimensionality of the electronlike Fermi surfaces is greatly enhanced, resulting in a better nesting behavior. Our study should be relevant to the recently reported superconducting phase $K_{0.5+x}Fe_{1.75+y}Se_2$ with both x and y being very tiny.

DOI: 10.1103/PhysRevB.87.161105 PACS number(s): 75.25.−j, 71.20.−b, 71.18.+y

Introduction. The discovery of vacancy-ordered iron selenides[1–4] has greatly stimulated the study of iron-based superconductors.[5] These compounds share a general chemical formula of $A_yFe_{2-x}Se_2$, and their crystal structures are close to $BaFe_2As_2$. However, they differ from the latter because the iron sites are not fully occupied in the selenides, and the iron vacancies may form ordered structures at certain x. For example, in the vacancy-ordered $K_{0.8}Fe_{1.6}Se_2$ (or $K_2Fe_4Se_5$, 245 phase), the iron vacancies form a superstructure of $\sqrt{5}\times\sqrt{5}$ (in units of nearest-neighbor iron-iron distance), separating square blocks of four iron atoms. The distinct geometry and the magnetic frustration thereafter lead to a unique antiferromagnetic (AFM) ground state pattern, i.e., the block-spin AFM.[3,6]

The presence of the ordered vacancy patterns alters the symmetry of the crystal lattice, and therefore its effect is far beyond the simple rigid-band shifting model. The new crystal symmetry modulates the electronic structure of the vacancy-free AFe_2Se_2 (or 122) phase, and the iron vacancies introduce extra scattering centers that further modify the electronic states. Such an effect of electronic structure reconstruction is absent in the vacancy-disordered compounds;[7,8] thus, the electronic structure of these vacancy-ordered phases can be completely different from one another, although their chemical composition may look fairly similar. It therefore leads to a question that among all the possible vacancy-ordered phases, which one is the actual parent phase for the superconductivity. As the 245 phase seems to be present universally in these superconducting samples, it was proposed that the pairing was mediated by AFM fluctuation in the doped 245 compound.[6,9] This argument was challenged by a phase-separation scenario that the 245 phase and the superconducting phase are spatially separated. The phase-separation argument has been supported by angle resolved photoemission spectroscope (ARPES)[10,11] and scanning tunneling microscope (STM) or transmission electron microscopy (TEM) experiments,[12–14] which suggest the vacancy concentration is much smaller and are disordered in the superconducting phase.[15]

Very recently, there has been an experimental report on $T_c = 33$ K superconducting iron selenides, which consists of superconducting bricks embedded in a background of 245 phase. The bricks have a chemical component $K_{0.5+x}Fe_{1.75+y}Se_2$. In these bricks, which take up about 20% of the volume, it is found that $x \approx 0.15$ and $y \approx 0.01$. This raises an interesting possibility that the vacancy-ordered $K_{0.5}Fe_{1.75}Se_2$ (278 phase hereafter) may be a parent compound of the superconducting phase.[16] The authors presented the preliminary verification of this possible parent phase by conducting self-consistent measurements of chemical compositions and the atomic imaging through scanning tunneling. Therefore, it will be interesting and urgent to provide first-principles calculations and theoretical studies on this 278 phase. Note that unlike the 245 phase, the single crystal 278 phase has yet to be discovered, and the phase form only "spider-web"-like filaments.

In this Rapid Communication, we present our latest first-principles results of the 278 phase. We examine the structural distortions induced by the iron vacancies, calculate its band structure and density of states, and compare them with the 122 phase. We present and compare its bare electronic susceptibility and nesting functions at zero and 0.1*e* doping levels. From these calculations, we conclude that the ground state for the 278 phase is stripelike AFM and metallic. Upon 0.1*e* electron doping, which quickly suppresses the long range AFM order, the two dimensionality of the Fermi surface sheets is greatly enhanced, resulting in a better nesting behavior.

Method. In the current study, we employed density functional theory (DFT) using the plane-wave basis as implemented in the Vienna *ab initio* simulation package (VASP).[17,18] The ion-valence electron interactions were modeled using the projected augmented wave (PAW) method, and the Perdew, Burke, and Ernzerhof flavor of exchange-correlation functional was chosen.[19] A 480 eV energy cutoff for the plane-wave basis and a $6\times6\times3$ Γ-centered K grid ensures the total energy converges less than 1 meV/atom. The lattice constants and internal atomic positions were fully optimized until forces on individual atoms are smaller than 1 meV/Å and the total stress is less than 0.05 kbar. The density of states (DOS) calculations were performed on a much denser K grid of $24\times24\times12$ and using the tetrahedra method.

The obtained band structure was then fitted to a tight-binding Hamiltonian of 70 Fe-3*d* orbitals using the maximally

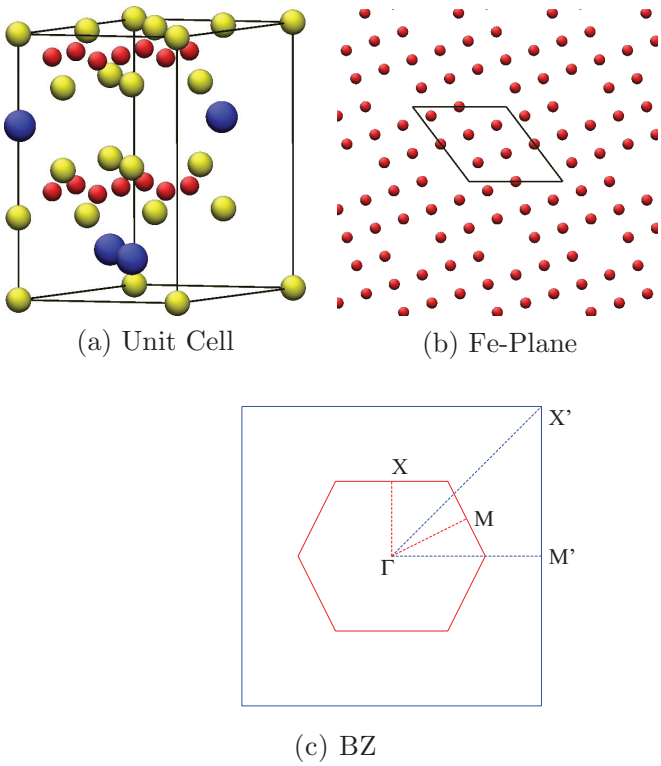

(a) Unit Cell (b) Fe-Plane

(c) BZ

FIG. 1. (Color online) (a) The unit cell of the 278 phase. The red atoms are iron, the blue atoms are potassium, and the yellow atoms are selenium. (b) The iron plane showing the ordered vacancies and the choice of lattice vectors as in (a). It is obvious that the two lattice vectors are both $\sqrt{10}$ (in units of nearest-neighbor Fe-Fe distance). (c) The first BZ (solid lines) and IBZ (dotted lines) of the 122 phase (the blue lines) and the 278 phase (the red lines). Both M' and X' in the 122 IBZ are X in the 278 IBZ.

projected Wannier function method.[20] The resulting Hamiltonian was then used to interpolate the electronic states on a dense Γ-centered $100 \times 100 \times 100\,K$ grid. The bare electronic susceptibility χ_0 is then calculated using

$$\chi_0(\mathbf{q}) = \frac{1}{N_\mathbf{k}} \sum_{mn} \sum_{\mu\nu\mathbf{k}} \frac{\langle m|\mu\mathbf{k}\rangle\langle\mu\mathbf{k}|n\rangle\langle n|\nu\mathbf{k}+\mathbf{q}\rangle\langle\nu\mathbf{k}+\mathbf{q}|m\rangle}{\epsilon_{\nu\mathbf{k}+\mathbf{q}} - \epsilon_{\mu\mathbf{k}} + i0^+} \times [f(\epsilon_{\mu\mathbf{k}}) - f(\epsilon_{\nu\mathbf{k}+\mathbf{q}})],$$

where $\epsilon_{\mu\mathbf{k}}$ and $f(\epsilon_{\mu\mathbf{k}})$ are the band energy (measured from E_F) and occupation number of $|\mu\mathbf{k}\rangle$, respectively, $|n\rangle$ denotes the nth Wannier orbital, and $N_\mathbf{k}$ is the number of $\mathbf{k}$ points used for the irreducible Brillouin zone (IBZ) integration. It is worth noting that one should not make the usual assumption that $\langle\mu\mathbf{k}|n\rangle = 1$, as pointed out by Graser *et al.*[21] The information is also used to calculate the nesting function using

$$f(\mathbf{q}) = \frac{1}{N_\mathbf{k}} \sum_{\mathbf{k}} \delta(\epsilon_{\mu\mathbf{k}})\delta(\epsilon_{\nu\mathbf{k}+\mathbf{q}}).$$

Results and discussion. Figures 1(a) and 1(b) show the unit cell we chose to perform our calculations. While the iron-vacancy order is crucial to the electronic structure of these compounds, the effect of potassium order seems to be negligible except for the resulting chemical potential shifting, as shown in previous studies.[3,4] Therefore, without losing generality, we chose a unit cell with high symmetry where the occupied potassium sites are closest to the iron-vacancy sites. Figure 1(c) compares the IBZ of a 122 phase unit cell (enclosed by blue dotted lines) and the one of a 278 phase unit cell (enclosed by red dotted lines). It is worth noting that the area of the first Brillouin zone (BZ) for the 122 phase (the blue square) is four times the one for the 278 phase (the red hexagon).

The optimized lattice constants for the 278 phase are $a = 8.3813$ Å and $c = 13.9846$ Å [Fig. 1(b)], respectively. Previous density functional studies of iron pnictides and iron selenides severely suffer from a c-collapse problem where the optimized lattice constant c is significantly smaller (beyond the usual DFT limit of 5%) than the experimental value. This particular problem is in fact absent in the 278 phase if one assumes that the 278 phase c value should not be too far from the 122 phase (14.0367 Å). The γ angle formed by the a and b lattice vectors is 127.12°, which is slightly larger than 126.87°. The latter is the ideal value of γ if the iron square lattices are perfectly preserved. Therefore, the square lattice of iron is slightly distorted by less than 0.5%. Furthermore, the optimized lattice constants can be roughly translated into $a' = 3.748$ Å in the 122 phase, which is 4.3% smaller than the experimental value, suggesting a contraction of lattice constants due to the vacancy ordering. The presence of the ordered vacancies also introduces further distortions of the atomic positions within one unit cell. The seven iron sites in one unit cell split into three nonequivalent classes: the four iron atoms that are nearest neighbors of the iron vacancy (Fe^{I}), the iron site that is in between two neighboring iron vacancies (Fe^{II}), and the rest the two iron atoms (Fe^{III}); their fractional heights are 0.2488, 0.2463, and 0.2523, respectively. In addition, the Fe^{I} atoms slightly move towards the nearest vacancy site while both Fe^{II} and Fe^{III} remain in the square lattice position (so that they only displace in the z direction). The Fe-Se-Fe angles formed by the next-nearest-neighbor iron sites and the above selenium atom are in the range of 108.16°–109.66°, slightly larger than the one in the KFe_2Se_2 122 phase (106.61°).

With the optimized crystal structure, we then study its electronic structure. Figures 2(a) and 2(b) show the band structure and density of states (DOS) of the 278 phase. As the unit cell of the 278 phase is eight times the 122 phase primitive cell (which is not orthogonal), its irreducible Brillouin zone (IBZ) as well as the band structure is heavily folded [for the IBZ folding, please refer to Fig. 1(c)]. However, it can still be identified that three bands cross the Fermi level, suggesting three Fermi surface sheets in the BZ. Unlike either the 122 or 245 phase, the Fe-3d bands in the 278 phase are well separated from all other contributions, and dominate the electronic states from $E_F - 3.0$ eV to $E_F + 2.0$ eV, as suggested in the projected DOS calculations [Fig. 2(b)]. Several flat bands can be identified close to E_F, from Γ to M and from Z to A, which contribute the DOS peak at E_F. It is worth noting that the flat band contribution to conductivity is almost negligible due to the large effective mass. Thus, the pseudogaplike feature from $E_F - 1.0$ eV to $E_F + 1.0$ eV may be consistent with the "bad-metal" behavior observed in the experiments.

As the electronic states near E_F are almost exclusively contributed by the Fe-3d orbitals, we can easily fit its band

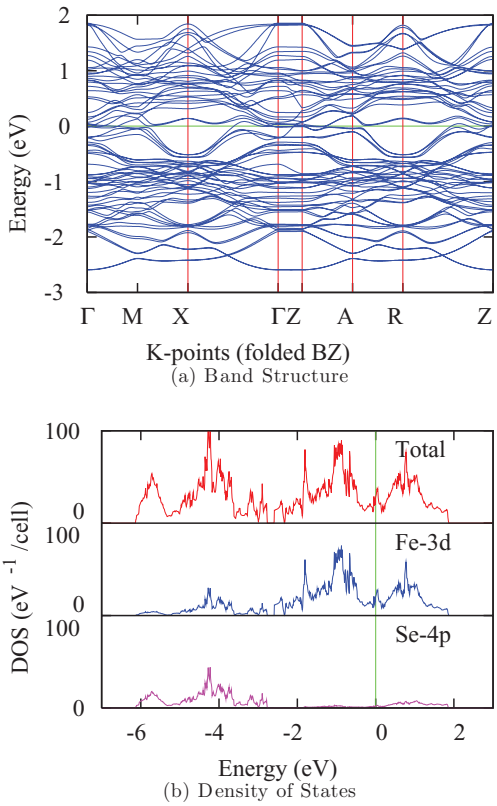

FIG. 2. (Color online) (a) Band structure and (b) density of states of the 278 phase. Unlike other iron pnictides or chalcogenides, the electronic states of the 278 phase from $E_F - 3.0$ eV to $E_F + 2.0$ eV are almost exclusively from the Fe-3d orbitals.

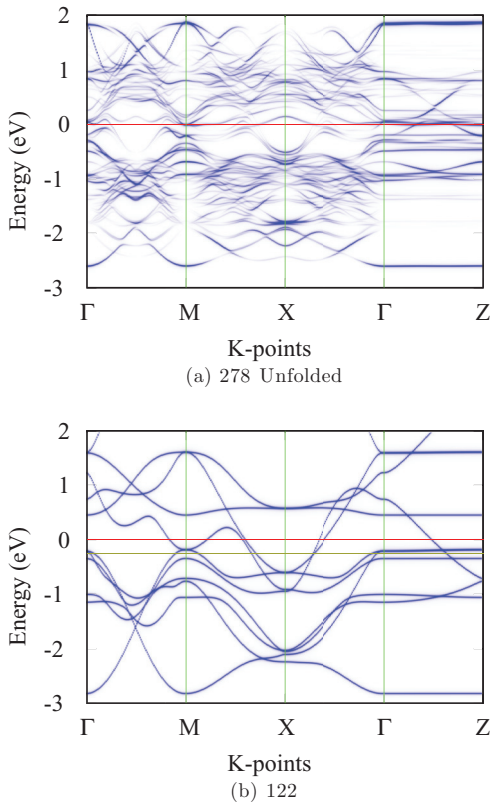

FIG. 3. (Color online) Band structure of (a) the 278 phase in the unfolded BZ (122 phase BZ), and (b) the 122 phase in the 122 phase BZ. In both figures, the Fermi level E_F is aligned at zero energy (red line), while in the 122 phase plot, an additional -0.25 eV line (corresponding to the doping level in the 278 phase) is shown.

structure within $E_F - 3.0$ eV to $E_F + 2.0$ eV to a tight-binding Hamiltonian using maximally projected Wannier orbitals. The original 278 phase band structure is then unfolded to the 122 phase IBZ using the method introduced by Ku *et al.*[22] The resulting unfolded band structure is shown in Fig. 3(a) in comparison with the 122 phase band structure [Fig. 3(b)]. Due to the strong structural distortion and iron vacancies, the band structure of the 278 phase is significantly smeared out, although some features of the latter can still be identified from the unfolded 278 band structure. In particular, both the upper and lower band limit of the Fe-3d orbitals seem to be shifted $\sim$0.25 eV, meaning the Fermi level E_F of the 278 phase is shifted ~ -0.25 eV. It is worth noting that this shifting of E_F corresponds to $\sim 0.5|e|$ hole doping in the 122 unit cell, or $K_{0.75}Fe_2Se_2$ in the chemical formula. A similar effective doping feature was also previously identified in the 245 phase.[8] One can also identify some other characteristic rigid-band shifting in the unfolded 278 phase band structure, especially along Γ-Z, since the direction is mostly unaffected by the iron vacancies whose effect is primarily in plane.

Features beyond rigid-band shifting can also be identified in the unfolded band structure. First of all, the additional scattering centers caused significant band smearing and splitting in the regions around $E_F - 1.0$ eV and $E_F + 1.0$ eV, similar to the unfolded band structure of the 245 phase.[8] Second, the -0.25 eV Fermi level shifting allows two holelike Fermi surface sheets to emerge around Γ in the 122 phase, as one can clearly identify two holelike band dispersions crossing the -0.25 eV line in Fig. 3(b). This feature, however, is absent in the 278 phase band structure. Another shallow holelike band crossing, however, can be identified around X in the 278 phase unfolded band structure, which is clearly missing in the rigid-band shifted 122 phase. Finally, the bands around E_F are extremely smeared out except from Γ to Z, suggesting that the electron transport suffers from strong scattering in the a-b plane and may exhibit a low conductivity. Due to the complexity of the band structure, it is rather difficult to conclude which is the major carrier, but both the electron and hole seem to play roles.

The bare electronic susceptibility χ_0 is also calculated using the maximally projected Wannier function Hamiltonian. Figures 4(a) and 4(b) show χ_0 at the $k_z = 0$ plane for both the parent 278 phase and 0.1e-doped phase, respectively. Previous calculations for $BaFe_2As_2$ and LaOFeAs (Refs. 23 and 24) show significant enhancement at $(\pi,0)$ in the two-iron (unfolded) BZ. For the parent 278 phase, a similar enhancement of $\sim$100% can also be identified around (π,π) in the folded BZ, suggesting an AFM long range order. In fact, mean-field calculations based on the extended J_1-J_2 model have proposed four possible ground state candidates.[25] By employing spin-polarized density functional calculations, we confirm that the ground state parent 278 phase is stripelike order AFM, which is $\sim$150 meV/Fe lower than the nonmagnetic phase and $\sim$30 meV/Fe lower than the second lowest AFM order. With 0.1e electron doping, the enhancement is greatly reduced

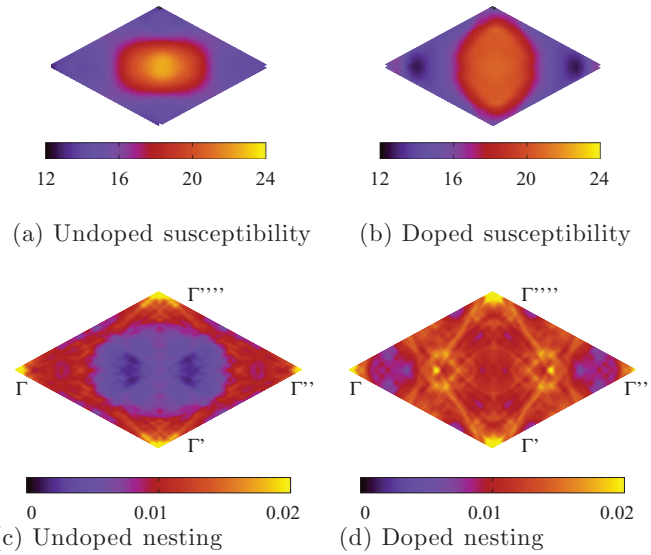

(a) Undoped susceptibility (b) Doped susceptibility

(c) Undoped nesting (d) Doped nesting

FIG. 4. (Color online) (a), (b) Bare electron susceptibility χ_0 and (c), (d) nesting function f of parent 278 phase (a), (c) and the 0.1e electron-doped 278 phase (b), (d). The plots are made in a full BZ with Γ at four corners.

and broadened, and thus the long range AFM order may be destroyed at such a doping level.

Finally, we present the Fermi surfaces for both the parent compound and the 0.1e-doped compound (Fig. 5). As pointed out previously, despite the complexity of the band structure of the 278 phase, only three bands cross the Fermi level, forming three Fermi surface sheets. Upon electron doping, the sizes of the two hole pockets along Γ-M are dramatically reduced while the electron pockets are greatly enlarged. Apart from that, a fourth sheet emerges around Γ. Furthermore, the two dimensionality of both electron pockets is significantly enhanced, leading to a better nesting behavior. This is also reflected in the nesting function plots [Figs. 4(c) and 4(d)], which show over a two times enhancement of the nesting function around the center of the BZ.

Conclusion. In conclusion, we have performed a first-principles study on vacancy-ordered $K_{0.5}Fe_{1.75}Se_2$

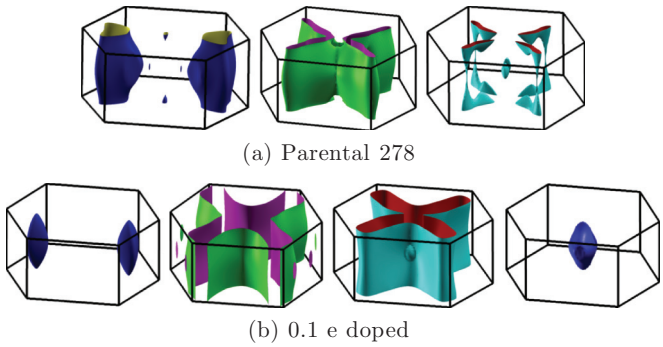

(a) Parental 278

(b) 0.1 e doped

FIG. 5. (Color online) Fermi surface sheets of (a) the parent 278 phase and (b) the 0.1e electron-doped 278 phase. The Γ point is at the center of each plot.

(278 phase). The ground state of the parent 278 phase is stripelike AFM and metallic, whose magnetic order may be destroyed by electron and/or hole doping. The Fe-3d orbitals dominate the electron DOS near the Fermi level, and both electron- and holelike Fermi surfaces emerge in the BZ. The unfolded band structure shows limited features of a hole-doped 122 phase, but effects beyond the rigid-band model must be taken into consideration to understand the electronic structure of the 278 phase. Finally, a 0.1e electron doping significantly enhances the two dimensionality of its Fermi surfaces, resulting in a better nesting behavior. In our present calculations, electron correlations beyond the local density approximation level have been neglected. A strong on-site Coulomb repulsion could alter the magnetic order and lead to a Mott insulator, in light of the AFM Mott insulator in the 245 compound. The analysis is beyond the scope of the present Rapid Communication and an experimental synthesis of the 278 phase would shed light on this issue.

Acknowledgments. We would like to thank H.-H. Wen for sharing the experimental results and useful discussions. This work has been supported by the NSFC (No. 11274006 and No. 11274269) and the NSF of Zhejiang Province (No. LR12A04003). All calculations were performed at the High Performance Computing Center of Hangzhou Normal University College of Science.

*ccao@hznu.edu.cn
†fuchun@hku.hk

[1] J. Guo, S. Jin, G. Wang, S. Wang, K. Zhu, T. Zhou, M. He, and X. Chen, Phys. Rev. B **82**, 180520 (2010).
[2] M.-H. Fang, H.-D. Wang, C.-H. Dong, Z.-J. Li, C.-M. Feng, J. Chen, and H. Q. Yuan, Europhys. Lett. **94**, 27009 (2011).
[3] C. Cao and J. Dai, Phys. Rev. Lett. **107**, 056401 (2011).
[4] X.-W. Yan, M. Gao, Z.-Y. Lu, and T. Xiang, Phys. Rev. Lett. **106**, 087005 (2011).
[5] Y. Kamihara, T. Watanabe, M. Hirano, and H. Hosono, J. Am. Chem. Soc. **130**, 3296 (2008).
[6] W. Bao, Q.-Z. Huang, G.-F. Chen, M. A. Green, D.-M. Wang, J.-B. He, and Y.-M. Qiu, Chin. Phys. Lett. **28**, 086104 (2011).
[7] T. Berlijn, P. J. Hirschfeld, and W. Ku, Phys. Rev. Lett. **109**, 147003 (2012).
[8] C.-H. Lin, T. Berlijn, L. Wang, C.-C. Lee, W.-G. Yin, and W. Ku, Phys. Rev. Lett. **107**, 257001 (2011).
[9] Y.-Z. You, F. Yang, S.-P. Kou, and Z.-Y. Weng, Phys. Rev. Lett. **107**, 167001 (2011).
[10] T. Qian, X.-P. Wang, W.-C. Jin, P. Zhang, P. Richard, G. Xu, X. Dai, Z. Fang, J.-G. Guo, X.-L. Chen *et al.*, Phys. Rev. Lett. **106**, 187001 (2011).
[11] Y. Zhang, L. X. Yang, M. Xu, Z. R. Ye, F. Chen, C. He, H. C. Xu, J. Jiang, B. P. Xie, J. J. Ying *et al.*, Nat. Mater. **10**, 273 (2011).
[12] W. Li, H. Ding, P. Deng, K. Chang, C. Song, K. He, L. Wang, X. Ma, J.-P. Hu, X. Chen *et al.*, Nat. Phys. **8**, 126 (2012).
[13] W. Li, H. Ding, Z. Li, P. Deng, K. Chang, K. He, S. Ji, L. Wang, X. Ma, J.-P. Hu *et al.*, Phys. Rev. Lett. **109**, 057003 (2012).
[14] Z. Wang, Y. J. Song, H. L. Shi, Z. W. Wang, Z. Chen, H. F. Tian, G. F. Chen, J. G. Guo, H. X. Yang, and J. Q. Li, Phys. Rev. B **83**, 140505 (2011).

[15] Y. Zhou, D.-H. Xu, F.-C. Zhang, and W.-Q. Chen, Europhys. Lett. **95**, 17003 (2011).

[16] X. Ding, D. Fang, Z. Wang, H. Yang, J. Liu, Q. Deng, G. Ma, C. Meng, Y. Hu, and H.-H. Wen, arXiv:1301.2668.

[17] G. Kresse and J. Hafner, Phys. Rev. B **47**, 558 (1993).

[18] G. Kresse and D. Joubert, Phys. Rev. B **59**, 1758 (1999).

[19] J. P. Perdew, K. Burke, and M. Ernzerhof, Phys. Rev. Lett. **77**, 3865 (1996).

[20] To do this, we used the WANNIER90 code without performing the optimization procedure. As pointed out in Ref. 22, the optimization procedure may alter the symmetry of the Wannier orbitals, leading to potential problems in the band structure unfolding process later on.

[21] S. Graser, T. A. Maier, P. J. Hirschfeld, and D. J. Scalapino, New J. Phys. **11**, 025016 (2009).

[22] W. Ku, T. Berlijn, and C.-C. Lee, Phys. Rev. Lett. **104**, 216401 (2010).

[23] I. I. Mazin, D. J. Singh, M. D. Johannes, and M. H. Du, Phys. Rev. Lett. **101**, 057003 (2008).

[24] S. Graser, A. F. Kemper, T. A. Maier, H.-P. Cheng, P. J. Hirschfeld, and D. J. Scalapino, Phys. Rev. B **81**, 214503 (2010).

[25] F. Lu *et al*. (private communication).